



OPEN

Temperature-dependent Fermi surface probed by Shubnikov–de Haas oscillations in topological semimetal candidates DyBi and HoBi

Paulina Nowakowska, Orest Pavlosiuk✉, Piotr Wiśniewski & Dariusz Kaczorowski

Rare earth-based monpnictides are among the most intensively studied groups of materials in which extremely large magnetoresistance has been observed. This study explores magnetotransport properties of two representatives of this group, DyBi and HoBi. The extreme magnetoresistance is discovered in DyBi and confirmed in HoBi. At $T = 2$ K and in $B = 14$ T for both compounds, magnetoresistance reaches the order of magnitude of $10^4\%$. For both materials, standard Kohler's rule is obeyed only in the temperature range from 50 to 300 K. At lower temperatures, extended Kohler's rule has to be invoked because carrier concentrations and mobilities strongly change with temperature and magnetic field. This is further proven by the observation of a quite rare temperature-dependence of oscillation frequencies in Shubnikov–de Haas effect. Rate of this dependence clearly changes at Néel temperature, reminiscent of a novel magnetic band splitting. Multi-frequency character of the observed Shubnikov–de Haas oscillations points to the coexistence of electron- and hole-type Fermi pockets in both studied materials. Overall, our results highlight correlation of temperature dependence of the Fermi surface with the magnetotransport properties of DyBi and HoBi.

Rare-earth monpnictides ($REPn$, where RE denotes one of the rare-earth elements and $Pn = As, Sb$ or Bi) have attracted broad scientific and technological interest due to their exceptional physical properties and potential applications in solar cells¹ thermoelectrics² plasmonics³ and spintronics⁴. In addition, the preparation of $RESb$ thin films has been developed^{5,6}, which may be important from the point of view of future applications.

Recently, interest in $REPn$ materials has surged due to the possible topologically non-trivial nature of their electronic bands⁷. In addition, unsaturated and extreme magnetoresistance (XMR), accompanied by magnetic field-induced low-temperature resistivity plateau, has been reported in many $REPn$ materials^{7–12}. At first, these phenomena in $LaSb$ have been attributed to the existence of topologically non-trivial electronic states⁷. However, alternative explanation that has been postulated for many $REPn$ compounds is perfect or nearly-perfect compensation of charge carriers^{8,12–17}. In order to experimentally verify the presence of topologically non-trivial states in $REPn$ compounds, their electronic structure has been studied directly by angle-resolved photoemission spectroscopy (ARPES). In $LaBi$, for example, several groups have found the presence of topologically non-trivial states of different natures: nodal-lines¹⁸, surface states^{10,19,20}, and multiple Dirac cones²¹. In addition, pressure-induced superconductivity has been reported for $LaBi$ and YBi ^{22,23}, which established them as possible topological superconductors, potentially hosting Majorana fermions.

The presence of a rare-earth element with partially filled f -shells in $REPn$ compounds provides even more fascinating physical properties. $PrBi$ has been reported to exhibit nontrivial Berry phase and quadrupolar moment²⁴, whereas topological quantum phase transition has been proposed in $HoSb$ ²⁵. Several antiferromagnets among $REPn$ family have been reported to demonstrate XMR^{12,15,26,27}. Interestingly, it has been proposed that within $RESb$ and $REBi$ series topological phase transitions could occur close to $SmSb$ and $DyBi$, respectively²⁸. Intriguing new magnetic splitting effect has recently been discovered in $NdBi$ ⁴ and other $REBi$ compounds²⁹. This splitting takes place below the Néel temperature (T_N) and leads to the appearance of new sheets of the Fermi

Institute of Low Temperature and Structure Research, Polish Academy of Sciences, Okólna 2, 50-422 Wrocław, Poland. ✉email: o.pavlosiuk@intibs.pl

surface, hole- and electron-like “magnetic” Fermi arcs, and it can lead to a change in the shape of the bulk Fermi pockets. Interestingly, these arcs can be topologically non-trivial in nature⁴.

We hypothesized that this behavior could be reflected in the properties of quantum oscillations (the appearance of new frequencies and the change in frequency with changing temperature), since the oscillation frequency is directly proportional to the cross-sectional area of the Fermi pocket³⁰. In NdBi, $T_N = 24$ K⁴, a temperature too high for quantum oscillations to be observed in this material. Therefore, in order to examine our conjecture, we chose two other REBi compounds with significantly lower T_N : DyBi ($T_N = 11.2$ K³¹) and HoBi ($T_N = 5.7$ K³²), and investigated their magnetotransport properties. HoBi has previously been reported to exhibit XMR, magnetic-field induced resistivity plateau and complex magnetic structure^{33–35}, which we also confirmed in our study. In contrast to HoBi, magnetotransport properties of DyBi were not studied. We found that, similar to HoBi, DyBi exhibits XMR and magnetic field-induced resistivity plateau. In addition, we observed that oscillation frequencies change with temperature variation in both compounds, which corresponds to a change in the topology of Fermi surface.

Results and discussion

Electrical resistivity

In zero magnetic field, the temperature dependence of electrical resistivity, $\rho(T)$, of both compounds (see Fig. 1 a,b) displays metallic-like behavior, with ρ decreasing as the temperature decreases, with values of $\rho = 25.6 \mu\Omega$ cm and $\rho = 40.2 \mu\Omega$ cm at $T = 300$ K for HoBi and DyBi, respectively. At $T = 2$ K electrical resistivity falls to $\rho = 0.46 \mu\Omega$ cm and $\rho = 0.63 \mu\Omega$ cm, for HoBi and DyBi, respectively (and residual resistivity ratios [$\equiv \rho(300 \text{ K})/\rho(2 \text{ K})$] are 56 and 64). A significant drop in electrical resistivity is observed as the temperature decreases below $T = 5.9$ K for HoBi and $T = 12$ K for DyBi. These drops can be attributed to the elimination of spin-disorder scattering by the antiferromagnetic ordering, which according to the literature takes place at $T_N = 5.7$ K and $T_N = 11$ K for HoBi and DyBi, respectively^{31,35,36}. Magnetic field of 14 T, applied transverse to the current, dramatically changes the $\rho(T)$ dependence: resistivity is enhanced in whole temperature range, and displays metallic-like behavior down to 60 K and 40 K, for HoBi and DyBi, respectively, followed by a sharp increase of ρ with further decreasing temperature. At low temperatures magnetic field-induced resistivity plateaus are observed (see insets to Fig. 1a,b) for both compounds. Similar behavior of $\rho(T)$ dependence has been reported in other rare earth bismuthides and antimonides: LuSb, LuBi, YBi, LaBi, LaSb, YSb, PrBi, GdSb, TbSb^{8–12,16,27}, and in several topological semimetals: ZrSiS, NbP, TaAs^{37–39}. Appearance of the magnetic field-induced resistivity plateau has been attributed to the metal-insulator transition^{40,41}, perfect or nearly perfect carrier compensation^{42,43} or Lifshitz transition⁴⁴. In most of RESb and REBi compounds, the overall $\rho(T)$ dependence in applied magnetic field (including resistivity plateau and change of behaviour from metallic- to semiconducting-like) has been described in terms of carrier compensation^{8–10,13,14,16,43}. For HoBi, the shape of $\rho(T)$ obtained in $B = 14$ T is similar to that of temperature dependent Hall coefficient ($R_H(T)$) obtained for $B = 14$ T, shown in the inset to Fig. 4.

Magnetoresistance

Figure 2 shows magnetoresistance, $MR = 100\% \times [\rho(B) - \rho(0)]/\rho(0)$ as a function of magnetic field applied transverse to the current, measured at several temperatures. Both compounds exhibit extremely large, positive and non-saturating MR, reaching (at $T = 2$ K, in $B = 14$ T) $2.2 \times 10^4\%$ and $1.3 \times 10^4\%$ for HoBi and DyBi, respectively. With increasing temperature MR gradually decreases, down to 11.3% and 8.6% for HoBi and DyBi, respectively (at $T = 300$ K and in $B = 14$ T). The MR values which we obtained for HoBi are slightly smaller than those reported in literature for this material, but the order of magnitude of MR is the same³⁴. In case of DyBi, the magnitude of MR is almost the same as that reported for DySb in Ref.²⁶. Values of MR in both compounds are related to the residual resistivity ratios in a similar way as in other REPN¹⁶. XMR exhibited by REPN series

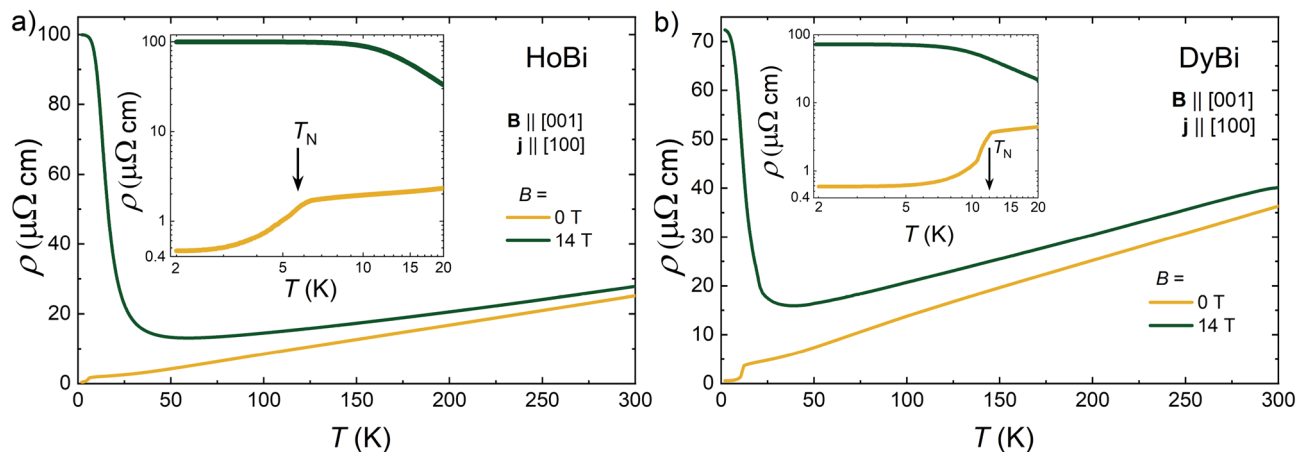


Figure 1. Temperature dependence of the electrical resistivity of HoBi (a) and DyBi (b), measured in zero magnetic field (yellow line) and in magnetic field of 14 T (green line), applied transverse to the electrical current (j) direction. Insets show the low-temperature data, with arrows indicating Néel temperatures.

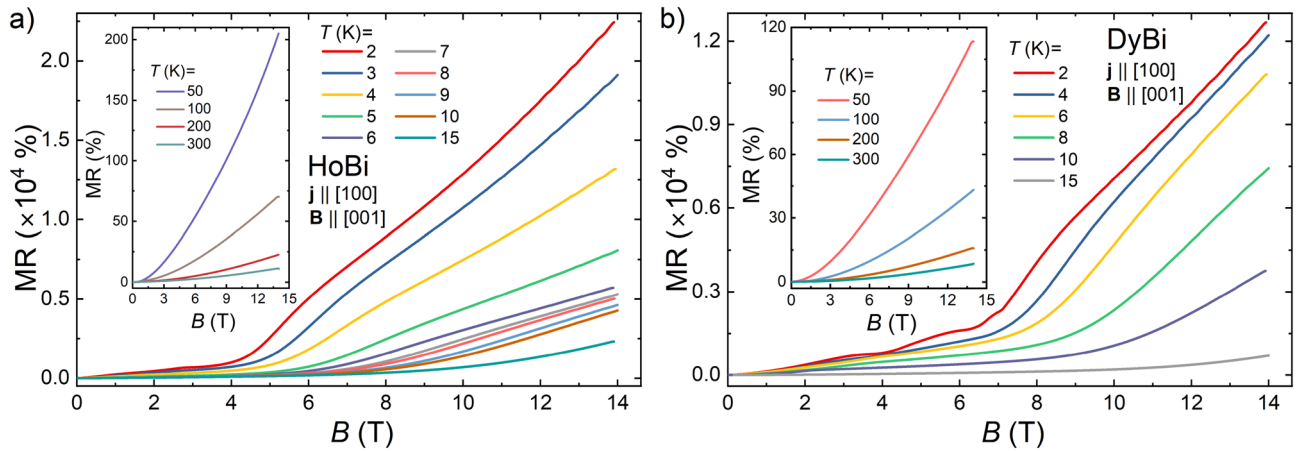


Figure 2. Transverse ($j \perp B$) magnetoresistance as a function of magnetic field for HoBi (a) and DyBi (b), measured at several temperatures.

has been attributed to: carrier compensation^{8,9,12,13,16,45}, metal-insulator transition⁷, or d - p orbital mixing in the presence of carrier compensation⁴⁶.

In numerous, both magnetic and non-magnetic $REPt$ demonstrating XMR, nearly quadratic behavior of $MR \propto B^m$ ($m < 2$) was observed^{12,47–49}. However, for HoBi and DyBi, $MR(B)$ isotherms for temperatures ≤ 15 K display strikingly different character. Those for $T < T_N$ exhibit two distinct regions, for example, at $T = 2$ K, in the low field region, $MR(B)$ increases with fluctuating slope up to about 5 T for HoBi, and up to about 8 T for DyBi. Such behavior can be related to series of metamagnetic transitions reported for both materials^{31,33–35,50}. Magnetic moments of Ho and Dy become fully aligned with the stronger magnetic field, and in such conditions the onset of typical $MR (\propto B^m)$ occurs in both compounds. Interestingly, our magnetotransport results for HoBi are in a full agreement with those reported by Wu et al.³⁴, although they differ from those described by Yang et al.³³ That difference comes from the magnetic anisotropy in HoBi, since in those measurements direction of the applied magnetic field was different ([001] and [110], respectively). In Ref.³³ it has been concluded that HoBi is the first material where XMR appears in the fully field-polarized magnetic state. Our results indicate that the mechanism of XMR in DyBi is the same as in HoBi.

It has recently been proposed that the magnetotransport properties of semimetals displaying XMR can be understood in the scope of Kohler’s scaling, which reflects the degree of charge carrier compensation⁵¹. According to standard Kohler’s rule $MR = (B/\rho_0)^m$, where m is a sample characteristic parameter, indicating the level of charge balance in the system. For a perfectly electron-hole compensated material $m = 2$. In order to test this approach for our materials, we performed the Kohler’s scaling, as shown in Fig. 3. Kohler’s rule is violated for both compounds from 2 to 15 K (see main panels of Fig. 3a,b), i.e. the temperature range covering antiferromagnetic order and noticeable short-range order. In several compounds exhibiting extreme magnetoresistance, e.g. LaBi, YBi, WP_2 , WTe_2 or TaAs, Kohler’s rule is violated as well^{39,44,52–54}, but in these cases violation is due to the change of concentration and mobility of carriers with temperature, not to the magnetic interactions. On the other hand, in the temperature interval from 50 to 300 K MR isotherms of HoBi and DyBi collapse onto a single curve (see insets to Fig. 3a,b). For the MR data obtained in the temperature range 50–300 K, the least-squares fitting (black

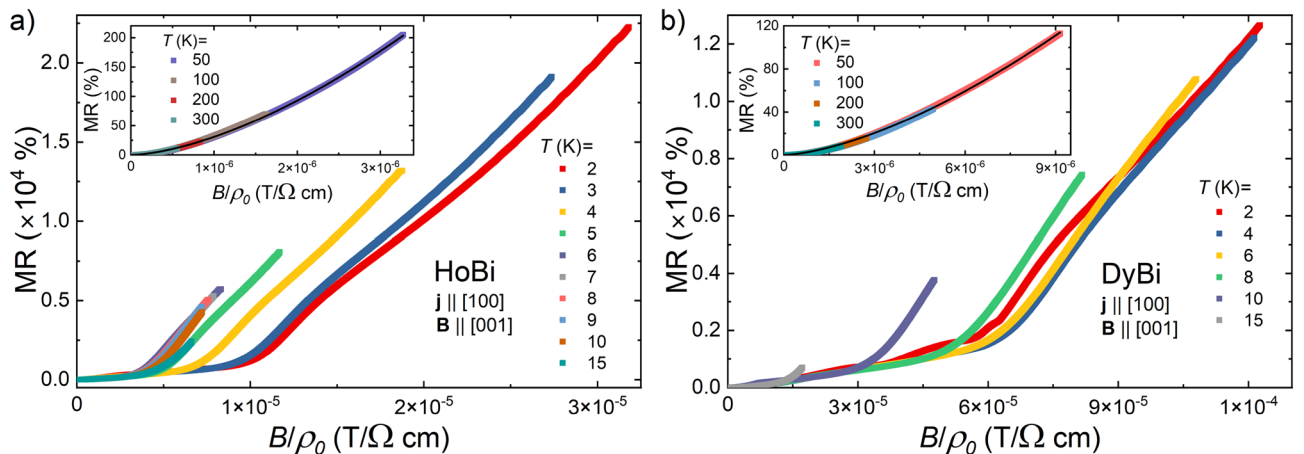


Figure 3. Standard Kohler’s scaling for HoBi (a) and DyBi (b). Main panels show the data taken in the temperature range 2–15 K; insets show the data recorded in the temperature range 50–300 K. Black solid lines in the insets correspond to the fits with Kohler’s formula.

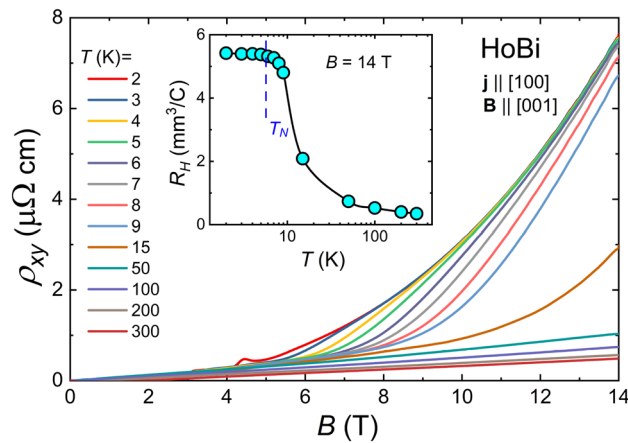


Figure 4. Hall resistivity (ρ_{xy}) of HoBi as a function of magnetic field taken at several different temperatures. Inset: temperature dependence of Hall coefficient in $B = 14$ T. Vertical dashed line indicates the Néel temperature.

solid lines in the insets to Fig. 3a,b) yielded $m = 1.6$ and $m = 1.54$, for HoBi and DyBi, respectively. Similarly, it has recently been shown that Kohler's scaling is effective at $T > 50$ K in HoSb and ErBi^{25,45}. For other *REPN* containing magnetic *RE*, Kohler's rule was disobeyed in the entire covered range of temperature^{12,27,34}. The magnitude of m that we obtained for both compounds is one of the smallest among *REPN*^{8,9,14,16,45,52}. To the best of our knowledge, the only material among *REPN* compounds with m smaller than we observed in this work is LaAs with $m = 1.35$ ⁵⁵.

The Kohler's rule is obeyed in simple non-magnetic metals, with one type of carriers and single scattering time⁵⁶ and in semimetals, only if mobilities of both types of carriers are small, and their ratio, as well as carrier concentrations are all temperature-independent⁵⁷. Therefore, violation of the Kohler's rule for HoBi and DyBi seems most likely due to the temperature-dependent carrier concentrations and/or mobilities. Results of the Hall effect data presented in Fig. 4 support such assumption. The Hall coefficient ($R_H = \rho_{xy}/B = 1/(en_H)$), which is inversely proportional to carrier concentration (n_H) varies strongly with increasing temperature (see inset to Fig. 4). Moreover, the frequency of observed Shubnikov–de Haas (SdH) oscillations also depend on temperature (see below), which is consistent with the assumption of temperature-dependent carrier concentrations in HoBi and DyBi.

Recently, an extended approach to Kohler's rule has been reported, $MR = (B/(n_T\rho_0))^m$ in which temperature-dependent carrier concentration is implemented through introducing a factor n_T ⁵⁸. We tested that approach to our data for temperatures where standard Kohler's scaling failed. We demonstrate the outcome in Fig. 5. For HoBi extended scaling is working, for $T \leq 15$ K all data above $MR \sim 5000\%$ collapse on single curve with $m = 1.7$. This exponent is different from 1.6 obtained for $T \geq 50$ K, which indicates small but clear change of electron-hole compensation between these two temperature ranges. In the case of DyBi extended scaling works, but the curve on which data collapse (for $4 < T < 6$ K, and $MR \sim 9000\%$) corresponds to $m = 1.85$, suggesting a higher degree of charge carriers compensation if compared with $T \geq 50$ K, for which $m = 1.54$. Parameter n_T strongly evolves

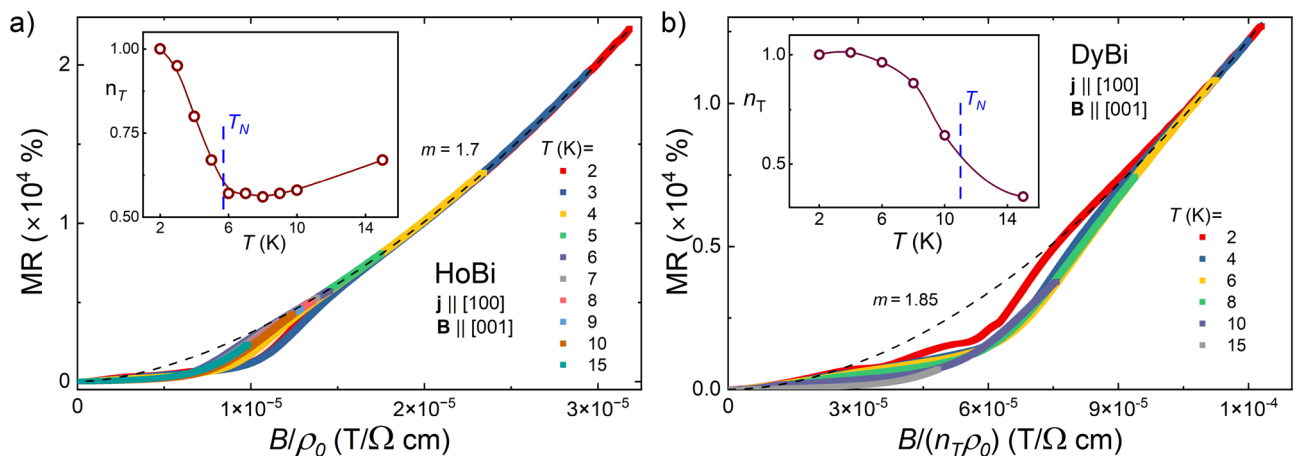


Figure 5. Extended Kohler's scaling, $MR = (B/(n_T\rho_0))^m$, for HoBi (a) DyBi (b); black dashed lines show power functions representing Kohler's rule. Insets show changes of the factor n_T with temperature (lines are guides for the eye). Blue dashed lines indicate the Néel temperatures.

with temperature, for both compounds, as shown in insets to Fig. 5a,b, implying a significant change of carrier concentration (we will discuss this further below when analyzing the SdH oscillations). In this range of T , strong interactions of magnetic moments, and series of metamagnetic transitions strongly influence scattering rate of charge carriers, and magnetoresistance regains its typical (power function) behavior only in strong magnetic fields, when antiferromagnetic order is destroyed and critical fluctuations damped.

Shubnikov–de Haas oscillations

Magnetoresistance isotherms, $MR(B)$, for both compounds show oscillatory behavior above $B = 9$ T, which we ascribe to the SdH effect. For both materials, the SdH oscillations survive at quite high temperatures, up to at least 10 K. Figures 6a, and 7a depict the oscillating part of the electrical resistivity ($\Delta\rho$) as a function of the inverse magnetic field ($1/B$), obtained by subtraction of a smooth background from the resistivity data. Fast Fourier transform (FFT) analysis of these oscillations revealed three fundamental frequencies (F_α , F_β and F_γ listed in Table 1), which points at possible complex form of Fermi pockets or/and at multi-band type of conductivity. F_i values we obtained for HoBi are very close to those reported in Ref.³³. In contrast to that report, we did not observe the high-frequency oscillations ($F > 900$ T), most probably due to the narrower range of magnetic field in which our experiments were carried out. For DyBi, our observation of the SdH oscillations is the first, and the frequencies we obtained (see Table 1) are quite close to those found for HoBi, which implies that relevant sheets of Fermi surfaces in both compounds are rather similar. According to the results of several theoretical

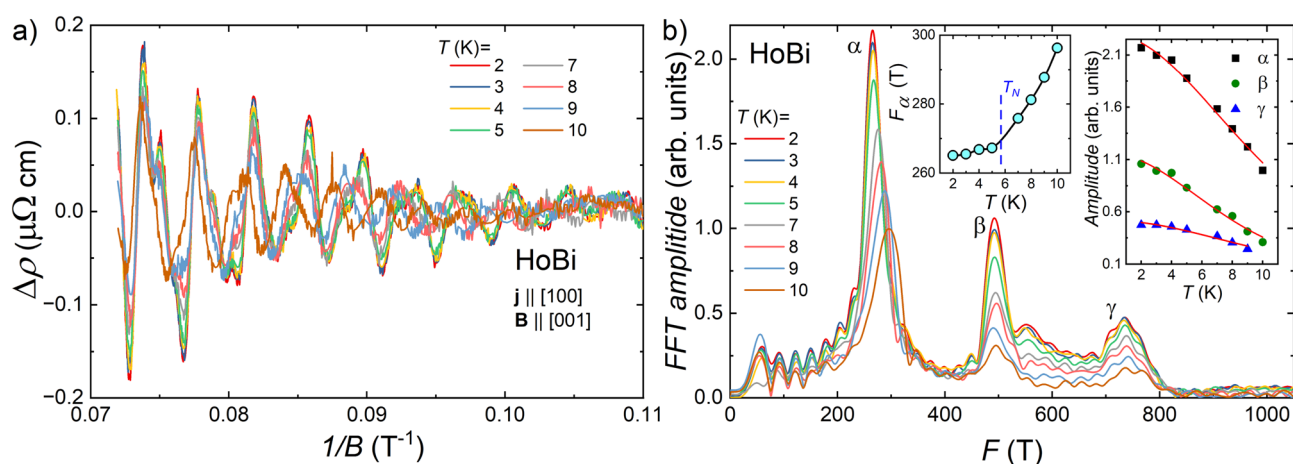


Figure 6. (a) The SdH oscillations extracted from electrical resistivity data in transverse magnetic field at different temperatures for HoBi. (b) Fast Fourier transform analysis of the data presented in (a). Left inset: amplitude of F_α principal frequency in FFT spectra as a function of temperature (black solid line is guide for the eye). Blue dashed line indicates the Néel temperature. Right inset: temperature dependence of the FFT peak height. Red solid lines represent the fits of Eq. (1) to the experimental data.

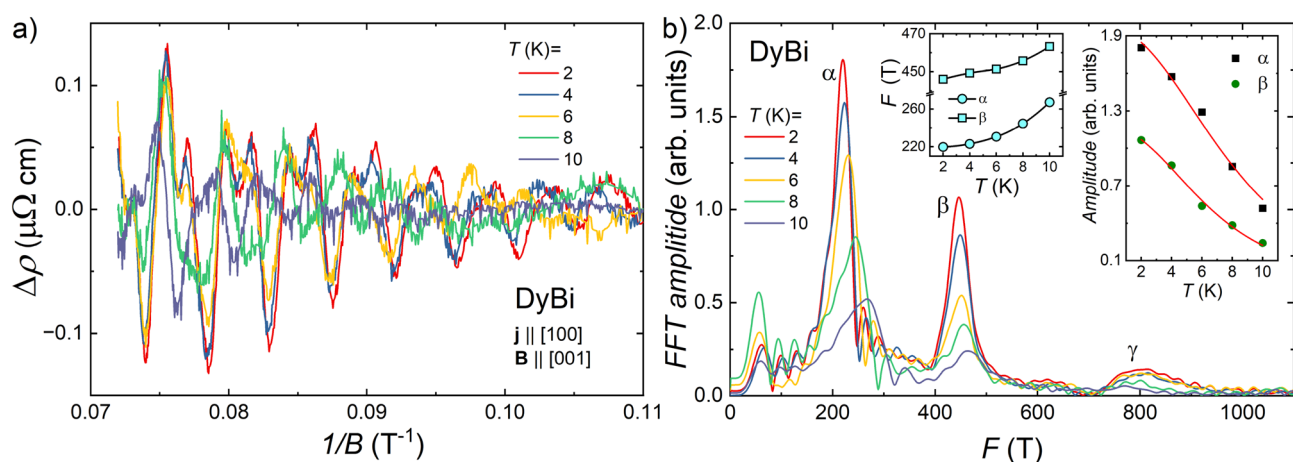


Figure 7. The SdH oscillations extracted from electrical resistivity data in transverse magnetic field at different temperatures for DyBi. (b) Fast Fourier transform analysis of the data presented in (a). Left inset: amplitudes of principal frequencies in FFT spectra as a function of temperature (black solid lines are guides for the eye). Right inset: temperature dependence of the FFT peak height. Red solid lines represent the fits of Eq. (1) to the experimental data.

Compound	$i =$	α	β	γ
HoBi (this work)	F_i (T)	265	492	735
	$k_{F,i}$ (\AA)	0.09	0.12	0.18
	n_i (cm^{-3})	2.44×10^{19}	9.22×10^{19}	
	m_i^* (m_e)	0.17	0.22	0.17
HoBi (Ref. ³³ , DFT calculations)	$F_{i,calc}$ (T)	243	489	835
	$m_{i,calc}^*$ (m_e)	1.14	0.54	0.46
HoBi (Ref. ³³ , SdH oscillations)	F_i (T)	280	513	747
	m_i^* (m_e)	0.27	0.29	0.29
DyBi (this work)	F_i (T)	220	446	815
	$k_{F,i}$ (\AA)	0.08	0.012	0.21
	n_i (cm^{-3})	1.85×10^{19}	9.74×10^{19}	
	m_i^* (m_e)	0.22	0.27	-
DySb (Ref. ²⁶ , DFT calculations)	$F_{i,calc}$ (T)	369	1022	1063
	$m_{i,calc}^*$ (m_e)	0.21	0.42	0.49
DySb (Ref. ²⁶ , SdH oscillations)	F_i (T)	369	745	1094
	m_i^* (m_e)	0.69	0.88	-

Table 1. Parameters obtained from the analysis of the Shubnikov–de Haas oscillations for HoBi and DyBi, compared to the data reported for HoBi in Ref.³³ and for DySb in Ref.²⁶.

calculations, Fermi surfaces of $REPn$ compounds, which contain heavy rare earth elements, are qualitatively similar, all of them possess two or three nearly isotropic hole-like pockets in the center of the Brillouin zone and strongly anisotropic triplicate electron-like pocket^{8,16,25–27,34,59–61}. In the magnetic-field induced polarized state (with all spins aligned with strong enough magnetic field) the electronic structure of magnetic $REPn$ changes with each Fermi pocket splitting into two pockets due to the magnetic-field induced time-reversal symmetry breaking^{25,27,33,34}. Such splitting has already been reported for HoBi^{33,34}. Comparing the frequencies we obtained to those reported in Ref.³³, we may assume that F_α originates from the smallest hole-like Fermi pocket (denoted as h_1 in Ref.³³); F_β and F_γ come from two extreme cross-sections of the electron-like pocket (denoted as e_2 in Ref.³³). For another $REPn$, DySb, quantum oscillations were also reported²⁶ and their frequencies are listed in Table 1 along those theoretically calculated. The authors of Ref.²⁶ ascribed the frequencies F_α and F_γ to the electron-like Fermi pocket and frequency F_β to the hole-like pocket. This assignment is different from that made for HoBi in Ref.³³. To find which option is valid for HoBi and DyBi, it might be necessary to perform angle-dependent studies of quantum oscillations and to calculate electronic structures for both materials.

According to the Onsager relation, oscillation frequencies are directly proportional to the area of the extreme cross-sections (S_i) of Fermi surface pockets: $F_i = (hS_i)/e$, where h stands for the Planck constant, and e is the elementary charge³⁰. Assuming, that shapes of hole-like and electron-like Fermi pockets of both compounds can be approximated by a sphere and an ellipsoid, respectively, we calculated the corresponding Fermi wave vectors (k_F) and charge carrier concentrations ($n = V_F/(4\pi^3)$, where V_F is volume of the Fermi pocket). The calculated values (listed in Table 1), are smaller than those obtained from our Hall effect results, as well as reported in literature³⁴. This difference is most likely due to the fact that not all Fermi pockets were detected with the SdH oscillations.

Interestingly, in the FFT spectra for both compounds, clear shifts of the peaks related to the F_α were observed. In the case of DyBi, the pronounced shift was also noticed for F_β . To see it more clearly, the temperature dependence of F_i are shown in the left insets to Figs. 6b and 7b, where one can see that F_i increases with increasing temperature. Similar behavior has previously been noticed for several $REPn$, such as DySb²⁶, SmBi⁶², HoSb⁶³, and NdSb⁴⁷. In the first three reports, the authors did not comment on these observations, while in the fourth one concluded that it indicated the change of topology of the Fermi surface. Interestingly, for $REPn$ containing non-magnetic RE, there were no reports on the temperature dependence of oscillations' frequencies, which may point that magnetism is responsible for this behavior. From another point of view, it is also known that in semimetals with small Fermi pockets and small effective masses, the Fermi level can be shifted with increasing temperature, leading to changes in the Fermi surface³⁰. For our materials, the Fermi temperature ($T_F = E_F/k_B$) is much larger than temperatures at which SdH oscillations were observed, therefore we can exclude the above scenario. The thermal expansion of the material is another possible source of the Fermi level shift³⁰. In antiferromagnets, at temperatures close to the T_N thermal expansion very often demonstrates a drastic change^{64,65}, which was observed for HoBi as well³². However, thermal expansion as the only source of change of the Fermi surface can also be ruled out for the following reasons: (i) for HoBi above T_N thermal expansion does not change significantly, but F_α continues to increase; (ii) for DyBi both F_α and F_β increase with increasing temperature, but if a simple Fermi level shift would be the reason of this, then one of these frequencies should decrease and the other increase with increasing temperature, since we ascribe them to Fermi pockets of different type, electron- and hole-like. Very recently, it has been proposed that change of oscillation frequency can be a signature of Dirac bands⁶⁶, however, in this case magnitude of frequency change is two orders of magnitude smaller than we observed for DyBi and HoBi. It has recently been shown that in several $REPn$ compounds a new type of magnetic splitting leads to the appearance of additional Fermi arcs below T_N ^{4,29}, moreover, such splitting can change the

shape of the 3D Fermi surface. Our analysis of the SdH oscillations did not reveal new oscillation frequencies due to the Fermi arcs, but we can speculate that the strong temperature dependence of oscillation frequencies comes from a new type of magnetic splitting, especially because the rate of change of F with temperature is very different below and above T_N (cf. left inset to Fig. 6b). That splitting is also likely to underlay dramatic change in Kohler's scaling between paramagnetic and antiferromagnetic state of HoBi (cf. inset to Fig. 5a).

Recently, temperature variations of the oscillation frequency have been found in $\text{MnBi}_{2-x}\text{Sb}_x\text{Te}_4$, PrAlNi and CePtBi ^{67–69}. For $\text{MnBi}_{2-x}\text{Sb}_x\text{Te}_4$ this variation was attributed to the change in the field-induced magnetization⁶⁷, and for PrAlNi it has been proposed that spin polarization is responsible for this effect⁶⁸. We suppose, that the former explanation may also be reasonable for HoBi and DyBi. In turn, for CePtBi , this rare behavior was attributed to the temperature variation of $4f$ electrons hybridization⁶⁹. This explanation can be excluded in our case, as the electronic bands related to the $4f$ electrons are located much above the Fermi level in $\text{RE}Pn$ ²⁷.

In Ref.⁶⁹, the authors explained the possible role of the so-called background magnetization and its temperature dependence on the oscillation frequency. For CePtBi described in that paper, this effect has been rejected (because of opposite than expected change of F vs. T), but for our results it could be applicable. However, such mechanism would affect all observed frequencies in a similar way, whereas for HoBi the value of F_β does not change at all, in contrast to strong change of F_α . Moreover, in high fields, between 9 and 14 T, the magnetization is very close to saturation and weakly changes with temperature. These allow us to rule out the role of background magnetization.

Despite the fact that the Fermi surfaces in both compounds vary with temperature, we made a working assumption that the effective masses are almost temperature independent. This allowed us to use the Lifshitz–Kosevich theory for determining the effective masses³⁰. FFT peaks' amplitudes as a function of temperature are shown in the right insets to Figs. 6b and 7b for HoBi and DyBi, respectively. Effective masses (m_i^*) were obtained through least-square fitting with the equation representing thermal damping of SdH oscillations:

$$R_i(T) = (\lambda m_i^* T / B_{\text{eff}}) / \sinh(\lambda m_i^* T / B_{\text{eff}}), (i = \alpha, \beta) \quad (1)$$

where $B_{\text{eff}} = 2/(1/B_1 + 1/B_2) = 10.96$ T and $\lambda = 14.7$ T/K. The value of B_{eff} was obtained for $B_1 = 14$ T and $B_2 = 9$ T, limiting magnetic field range of the analysis. Obtained effective masses for HoBi and DyBi are listed in Table 1, these values are similar to those reported for other $\text{RE}Pn$ ^{8,33,63}.

Conclusions

We have performed a comprehensive study of magnetotransport properties of two XMR materials, DyBi and HoBi. While the magnetotransport properties that we observed for HoBi are in agreement with previous reports^{33,34}, no systematic studies of magnetotransport of DyBi have previously been reported. For both materials, we observed XMR of the order of $10^4\%$ and magnetic field-induced resistivity plateau at low temperatures. We found that standard Kohler's scaling is obeyed at temperature range from 50 to 300 K. On the other hand, satisfying the extended Kohler's rule at $T \leq 15$ K supports the variation of carrier concentration with temperature. The results of the Hall effect measurements and analysis of the SdH oscillations also confirmed the temperature dependent carrier concentrations. The rare change of quantum oscillation frequencies with temperature increasing was observed for both materials and could be attributed to the change of the Fermi surface shape due to the emergence of the new type of Fermi arcs below T_N , recently discovered for several $\text{RE}Pn$ ^{4,29}. This mechanism is strongly supported by the clear difference in both, $n_T(T)$ and $F(T)$ behaviour in temperatures below and above T_N . Similarly to other $\text{RE}Pn$, the SdH oscillations in both studied compounds show multi-frequency character, where one of the frequencies comes from the hole-type Fermi pocket and others from electron-type Fermi pocket. This suggests that electron-hole compensation can be responsible for XMR in these compounds.

Methods

Sample synthesis and characterization

High quality single crystals of REBi ($\text{RE} = \text{Ho, Dy}$) were synthesized by the self-flux growth method with the molar ratio of constituent elements RE (purity of 99.9 wt%) : Bi (purity of 99.9999 wt%) = 1 : 20. The charge was heated in sealed quartz ampule up to 1373 K, held for 24 h at this temperature and then cooled to 873 K with a step of 2 K/h. The excess of Bi flux was removed using a centrifuge. The largest among obtained single crystals had a size of $3 \times 3 \times 3$ mm³. The REBi single crystals oxidize easily in ambient atmosphere and decompose after several hours. Samples were examined at room temperature using X-ray powder diffraction (XPRD) technique on the X'pert Pro (PANalytical) diffractometer with $\text{Cu-K}\alpha$ radiation. The crystal structure refinement (by the Rietveld method) was performed using Fullprof software⁷⁰. The obtained lattice parameters ($a = 6.225$ Å and $a = 6.249$ Å for HoBi and DyBi, respectively) are in a good agreement with data reported in literature^{34,71}. The single crystals were oriented, and their quality was checked by the Laue method using the Laue-COS (Proto) system.

Electrical transport measurements

Electrical transport properties, including electrical resistivity, Hall effect and magnetoresistance, were measured using a four-probe method employing the Physical Property Measurement System (PPMS, Quantum Design). Measurements were carried out in the temperature range 2–300 K and in the magnetic fields up to 14 T, with ac electrical current flowing along [100] crystallographic direction.

Data availability

The data that support the findings of this study are available from the corresponding author upon reasonable request.

Received: 14 July 2023; Accepted: 13 December 2023

Published online: 20 December 2023

References

- Zide, J. M. *et al.* Increased efficiency in multijunction solar cells through the incorporation of semimetallic ErAs nanoparticles into the tunnel junction. *Appl. Phys. Lett.* **88**, 162103 (2006).
- Liu, X. *et al.* Properties of molecular beam epitaxially grown ScAs:InGaAs and ErAs:InGaAs nanocomposites for thermoelectric applications. *J. Cryst. Growth* **316**, 56–59 (2011).
- Krivoy, E. M. *et al.* Rare-earth monopnictide alloys for tunable, epitaxial, designer plasmonics. *ACS Photon.* **5**, 3051–3056 (2018).
- Schrunk, B. *et al.* Emergence of Fermi arcs due to magnetic splitting in an antiferromagnet. *Nature* **603**, 610–615 (2022).
- Inbar, H. S. *et al.* Epitaxial growth, magnetoresistance, and electronic band structure of GdSb magnetic semimetal films. *Phys. Rev. Mater.* **6**, L121201 (2022).
- Chatterjee, S. *et al.* Weak antilocalization in quasi-two-dimensional electronic states of epitaxial LuSb thin films. *Phys. Rev. B* **99**, 125134 (2019).
- Tafti, F. F., Gibson, Q. D., Kushwaha, S. K., Haldolaarachchige, N. & Cava, R. J. Resistivity plateau and extreme magnetoresistance in LaSb. *Nat. Phys.* **12**, 272 (2016).
- Pavlosiuk, O., Kleinert, M., Swatek, P., Kaczorowski, D. & Wiśniewski, P. Fermi surface topology and magnetotransport in semimetallic LuSb. *Sci. Rep.* **7**, 12822 (2017).
- Pavlosiuk, O., Swatek, P. & Wiśniewski, P. Giant magnetoresistance, three-dimensional Fermi surface and origin of resistivity plateau in YSb semimetal. *Sci. Rep.* **6**, 38691 (2016).
- Niu, X. H. *et al.* Presence of exotic electronic surface states in LaBi and LaSb. *Phys. Rev. B* **94**, 165163 (2016).
- Vashist, A., Gopal, R. K., Srivastava, D., Karppinen, M. & Singh, Y. Fermi surface topology and large magnetoresistance in the topological semimetal candidate PrBi. *Phys. Rev. B* **99**, 245131 (2019).
- Song, J. J. *et al.* Extremely large magnetoresistance in the antiferromagnetic semimetal GdSb. *J. Mater. Chem. C* **6**, 3026–3033 (2018).
- Ghimire, N. J., Botana, A. S., Phelan, D., Zheng, H. & Mitchell, J. F. J. *Phys. Condens. Matter* **28**, 235601 (2016).
- Kumar, N. *et al.* Observation of pseudo-two-dimensional electron transport in the rock salt-type topological semimetal LaBi. *Phys. Rev. B* **93**, 241106 (2016).
- Wu, Z. *et al.* Probing the origin of extreme magnetoresistance in Pr/Sm mono-antimonides/bismuthides. *Phys. Rev. B* **99**, 035158 (2019).
- Pavlosiuk, O., Swatek, P., Kaczorowski, D. & Wiśniewski, P. Magnetoresistance in LuBi and YBi semimetals due to nearly perfect carrier compensation. *Phys. Rev. B* **97**, 235132 (2018).
- Ye, L., Suzuki, T., Wicker, C. R. & Checkelsky, J. G. Extreme magnetoresistance in magnetic rare-earth monopnictides. *Phys. Rev. B* **97**, 081108 (2018).
- Feng, B. *et al.* Experimental observation of node-line-like surface states in LaBi. *Phys. Rev. B* **97**, 155153 (2018).
- Jiang, J. *et al.* Observation of topological surface states and strong electron/hole imbalance in extreme magnetoresistance compound LaBi. *Phys. Rev. Mater.* **2**, 024201 (2018).
- Lou, R. *et al.* Evidence of topological insulator state in the semimetal LaBi. *Phys. Rev. B* **95**, 115140 (2017).
- Nayak, J. *et al.* Multiple Dirac cones at the surface of the topological metal LaBi. *Nat. Commun.* **8**, 13942 (2017).
- Xu, C. Q. *et al.* Extreme magnetoresistance and pressure-induced superconductivity in the topological semimetal candidate YBi. *Phys. Rev. B* **99**, 024110 (2019).
- Tafti, F. F. *et al.* Tuning the electronic and the crystalline structure of LaBi by pressure: From extreme magnetoresistance to superconductivity. *Phys. Rev. B* **95**, 014507 (2017).
- He, X. *et al.* PrBi: Topology meets quadrupolar degrees of freedom. *Phys. Rev. B* **101**, 075106 (2020).
- Zhang, J.-M. *et al.* Topological quantum phase transition in the magnetic semimetal HoSb. *J. Mater. Chem. C* **9**, 6996–7004 (2021).
- Liang, D. D. *et al.* Extreme magnetoresistance and Shubnikov–de Haas oscillations in ferromagnetic DySb. *APL Mater.* **6**, 086105 (2018).
- Tang, F. *et al.* Anisotropic large magnetoresistance and Fermi surface topology of terbium monoantimonide. *Mater. Today Phys.* **24**, 100657 (2022).
- Duan, X. *et al.* Tunable electronic structure and topological properties of LnPn (Ln=Ce, Pr, Sm, Gd, Yb; Pn=Sb, Bi). *Commun. Phys.* **1**, 71 (2018).
- Kushnirenko, Y. *et al.* Rare-earth monopnictides: Family of antiferromagnets hosting magnetic Fermi arcs. *Phys. Rev. B* **106**, 115112 (2022).
- Shoenberg, D. *Magnetic Oscillations in Metals* (Cambridge University Press, 1984).
- Hulliger, F. Magnetic behavior of DyBi. *J. Magn. Magn. Mater.* **15–18**, 1243–1244 (1980).
- Hulliger, F., Ott, H. R. & Siegrist, T. Low temperature behaviour of HoBi. *J. Less-Common Met.* **96**, 263–268 (1984).
- Yang, H. Y. *et al.* Interplay of magnetism and transport in HoBi. *Phys. Rev. B* **98**, 045136 (2018).
- Wu, Z. M. *et al.* Multiple metamagnetism, extreme magnetoresistance and nontrivial topological electronic structures in the magnetic semimetal candidate holmium monobismuthide. *New J. Phys.* **21**, 093063 (2019).
- Fente, A. *et al.* Low temperature magnetic transitions of single crystal HoBi. *Solid State Commun.* **171**, 59–63 (2013).
- Wada, H., Imai, H. & Shiga, M. Low temperature specific heat of DyBi and ErBi. *J. Alloys Compd.* **218**, 73 (1995).
- Ali, M. N. *et al.* Butterfly magnetoresistance, quasi-2D Dirac Fermi surface and topological phase transition in ZrSiS. *Sci. Adv.* **2**, e1601742 (2016).
- Shekhar, C. *et al.* Extremely large magnetoresistance and ultrahigh mobility in the topological Weyl semimetal candidate NbP. *Nat. Phys.* **11**, 645 (2015).
- Sankar, R. *et al.* Crystal growth and transport properties of Weyl semimetal TaAs. *J. Phys. Condens. Matter* **30**, 015803 (2018).
- Singha, R., Pariari, A. K., Satpati, B. & Mandal, P. Large nonsaturating magnetoresistance and signature of nondegenerate Dirac nodes in ZrSiS. *Proc. Natl. Acad. Sci. USA* **114**, 2468 (2017).
- Li, Y. *et al.* Resistivity plateau and negative magnetoresistance in the topological semimetal TaSb₂. *Phys. Rev. B* **94**, 121115 (2016).
- Wang, Y. L. *et al.* Origin of the turn-on temperature behavior in WTe₂. *Phys. Rev. B* **92**, 180402 (2015).
- Xu, J. *et al.* Origin of the extremely large magnetoresistance in the semimetal YSb. *Phys. Rev. B* **96**, 075159 (2017).
- Wu, Y. *et al.* Temperature-Induced Lifshitz Transition in WTe₂. *Phys. Rev. Lett.* **115**, 166602 (2015).
- Fan, L.-Y. *et al.* Anisotropic and extreme magnetoresistance in the magnetic semimetal candidate erbium monobismuthide. *Phys. Rev. B* **102**, 104417 (2020).
- Tafti, F. F. *et al.* Temperature-field phase diagram of extreme magnetoresistance. *Proc. Natl. Acad. Sci. USA* **113**, E3475 (2016).
- Wang, Y. *et al.* Topological semimetal state and field-induced Fermi surface reconstruction in the antiferromagnetic monopnictide NdSb. *Phys. Rev. B* **97**, 115133 (2018).
- Hu, Y. J. *et al.* Extremely large magnetoresistance and the complete determination of the Fermi surface topology in the semimetal ScSb. *Phys. Rev. B* **98**, 035133 (2018).

49. Wu, F. *et al.* Anomalous quantum oscillations and evidence for a non-trivial Berry phase in SmSb. *NPJ Quantum Mater.* **4**, 20 (2019).
50. Zhao, J. *et al.* Multiple metamagnetic transitions induced by high magnetic field in DyBi. *Phys. Rev. B* **106**, 224412 (2022).
51. Wang, Y. L. *et al.* Origin of the turn-on temperature behavior in WTe₂. *Phys. Rev. B* **92**, 180402 (2015).
52. Sun, S., Wang, Q., Guo, P.-J., Liu, K. & Lei, H. Large magnetoresistance in LaBi: Origin of field-induced resistivity upturn and plateau in compensated semimetals. *New J. Phys.* **18**, 082002 (2016).
53. Qian, B. *et al.* Extremely large magnetoresistance in the nonmagnetic semimetal YBi. *J. Mater. Chem. C* **6**, 10020–10029 (2018).
54. Wang, A. *et al.* Large magnetoresistance in the type-II Weyl semimetal WP₂. *Phys. Rev. B* **96**, 121107 (2017).
55. Yang, H.-Y. *et al.* Extreme magnetoresistance in the topologically trivial lanthanum mononpnictide LaAs. *Phys. Rev. B* **96**, 235128 (2017).
56. Ziman, J. *Electrons and Phonons: The Theory of Transport Phenomena in Solids* (Oxford University Press, 2001).
57. Pavlosiuk, O., Falat, P., Kaczorowski, D. & Wiśniewski, P. Anomalous Hall effect and negative longitudinal magnetoresistance in half-Heusler topological semimetal candidates TbPtBi and HoPtBi. *APL Mater.* **8**, 111107 (2020).
58. Xu, J. *et al.* Extended Kohler's rule of magnetoresistance. *Phys. Rev. X* **11**, 041029 (2021).
59. Xie, W. *et al.* Magnetotransport and electronic structure of the antiferromagnetic semimetal YbAs. *Phys. Rev. B* **101**, 085132 (2020).
60. Kakihana, M. *et al.* Fermi surface properties of semimetals YSb, LuSb, YBi, and LuBi studied by the de Haas-van Alphen effect. *J. Phys. Soc. Jpn.* **88**, 044712 (2019).
61. Hosen, M. M. *et al.* Observation of gapped state in rare-earth mononpnictide HoSb. *Sci. Rep.* **10**, 12961 (2020).
62. Sakhya, A. P., Paulose, P. L., Thamizhavel, A. & Maiti, K. Evidence of nontrivial Berry phase and Kondo physics in SmBi. *Phys. Rev. Mater.* **5**, 054201 (2021).
63. Wang, Y.-Y., Sun, L.-L., Xu, S., Su, Y. & Xia, T.-L. Unusual magnetotransport in holmium monoantimonide. *Phys. Rev. B* **98**, 045137 (2018).
64. Pavlosiuk, O., Kleinert, M., Wiśniewski, P. & Kaczorowski, D. Antiferromagnetic order in the half-Heusler phase TbPdBi. *Acta Phys. Pol. A* **133**, 498 (2018).
65. Bud'ko, S. L. *et al.* Thermal expansion and magnetostriction of pure and doped RAgSb₂ (R = Y, Sm, La) single crystals. *J. Phys. Condens. Matter* **20**, 115210 (2008).
66. Guo, C. *et al.* Temperature dependence of quantum oscillations from non-parabolic dispersions. *Nat. Commun.* **12**, 6213 (2021).
67. Jiang, Q. *et al.* Quantum oscillations in the field-induced ferromagnetic state of MnBi_{2-x}Sb_xTe₄. *Phys. Rev. B* **103**, 205111 (2021).
68. Lyu, M. *et al.* Nonsaturating magnetoresistance, anomalous Hall effect, and magnetic quantum oscillations in the ferromagnetic semimetal PrAlSi. *Phys. Rev. B* **102**, 085143 (2020).
69. Goll, G. *et al.* Temperature-dependent Fermi surface in CeBiPt. *Europhys. Lett.* **57**, 233 (2002).
70. Rodriguez-Carvajal, J. Recent advances in magnetic structure determination by neutron powder diffraction. *Phys. B: Condens. Matter* **192**, 55–69 (1993).
71. Yoshihara, K., Taylor, J. B., Calvert, L. D. & Despault, J. G. Rare-earth bismuthides. *J. Less-Common Met.* **41**, 329–337 (1975).

Acknowledgements

This work was supported by the National Science Centre (Poland) under research Grant 2021/40/Q/ST5/00066. For the purpose of Open Access, the author has applied a CC-BY public copyright license to any Author Accepted Manuscript (AAM) version arising from this submission. O.P. is thankful to the Max Planck Institute for Chemical Physics of Solids for their hospitality and support during a part of the work on this project. We thank K. Dyk for performing powder X-ray diffractography.

Author contributions

D.K., P.W. and O.P. conceived the study; O.P. and P.N. conducted all the experiments; O.P., P.N. and P.W. analysed the results; O.P. and P.N. wrote the manuscript with inputs from all authors. All authors discussed the results and edited the manuscript.

Competing interests

The authors declare no competing interests.

Additional information

Correspondence and requests for materials should be addressed to O.P.

Reprints and permissions information is available at www.nature.com/reprints.

Publisher's note Springer Nature remains neutral with regard to jurisdictional claims in published maps and institutional affiliations.



Open Access This article is licensed under a Creative Commons Attribution 4.0 International License, which permits use, sharing, adaptation, distribution and reproduction in any medium or format, as long as you give appropriate credit to the original author(s) and the source, provide a link to the Creative Commons licence, and indicate if changes were made. The images or other third party material in this article are included in the article's Creative Commons licence, unless indicated otherwise in a credit line to the material. If material is not included in the article's Creative Commons licence and your intended use is not permitted by statutory regulation or exceeds the permitted use, you will need to obtain permission directly from the copyright holder. To view a copy of this licence, visit <http://creativecommons.org/licenses/by/4.0/>.

© The Author(s) 2023